ACS Infectious Diseases

pubs.acs.org/journal/aidcbc

Article

Broad Tricyclic Ring Inhibitors Block SARS-CoV-2 Spike Function Required for Viral Entry

Sneha Ratnapriya, Anthony R. Braun, Héctor Cervera Benet, Danielle Carlson, Shilei Ding, Carolyn N. Paulson, Neeraj Mishra, Jonathan N. Sachs, Courtney C. Aldrich, Andrés Finzi, and Alon Herschhorn*

Cite This: https://doi.org/10.1021/acsinfecdis.1c00658

Read Online

ACCESS | Metrics & More | Article Recommendations | Supporting Information

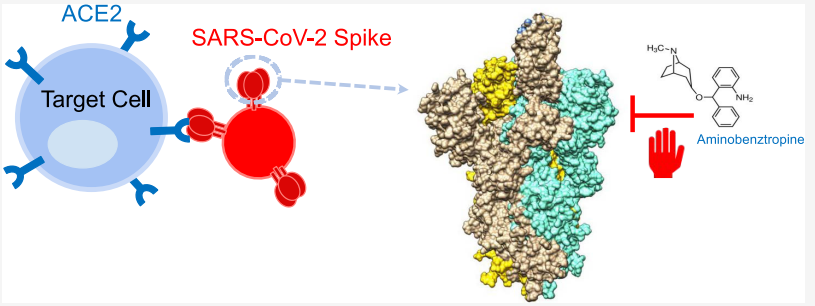

ABSTRACT: The entry of severe acute respiratory syndrome coronavirus 2 (SARS-CoV-2) into host cells requires binding of the viral spike glycoprotein to the angiotensin-converting enzyme 2 (ACE2) receptor, which triggers subsequent conformational changes to facilitate viral and cellular fusion at the plasma membrane or following endocytosis. Here, we experimentally identified selective and broad inhibitors of SARS-CoV-2 entry that share a tricyclic ring (or similar) structure. The inhibitory effect was restricted to early steps during infection and the entry inhibitors interacted with the receptor binding domain of the SARS-CoV-2 spike but did not significantly interfere with receptor (ACE2) binding. Instead, some of these compounds induced conformational changes or affected spike assembly and blocked SARS-CoV-2 spike cell−cell fusion activity. The broad inhibitors define a highly conserved binding pocket that is present on the spikes of SARS-CoV-1, SARS-CoV-2, and all circulating SARS-CoV-2 variants tested and block SARS-CoV spike activity required for mediating viral entry. These compounds provide new insights into the SARS-CoV-2 spike topography, as well as into critical steps on the entry pathway, and can serve as lead candidates for the development of broad-range entry inhibitors against SARS-CoVs.

KEYWORDS: *SARS-CoV-2, spike, small molecules, entry inhibitors, mode of action*

Worldwide spread of the severe acute respiratory syndrome coronavirus 2 (SARS-CoV-2), which causes the coronavirus disease 2019 (COVID-19), resulted in more than 4 million deaths to date.[1,2] The COVID-19 outbreak that began in Wuhan City, China in December 2019 has turned into a devastating pandemic and spread to more than 200 countries worldwide.[3] Two RNA-based vaccines and, more recently, vaccines delivered by different strains of non-replicating adenoviruses have been approved by the Food and Drug Administration (FDA) under emergency use authorization and are gradually administered to humans, significantly decreasing the morbidity and mortality associated with COVID-19.[4] Certain important aspects regarding the durability of the vaccines, reinfection, and the effectiveness in immunocompromised individuals and children are still under ongoing investigation.

Prevention measures are ideally complemented with effective therapeutics, but current treatment options are limited, highlighting the urgent need to understand and target critical steps in the replication of SARS-CoV-2. The entry of SARS-CoV-2 into host cells is mediated by the interaction of the viral spike on virions with the angiotensin-converting enzyme 2 (ACE2) receptor on target cells. Subsequent fusion of viral and cellular membranes can occur at the plasma membrane or following spike-mediated endocytosis of SARS-CoV-2 particles and requires proteolytic activation of the SARS-CoV-2 spike by a cellular protease prior to or after ACE2 binding. The SARS-CoV-2 spike is assembled on the viral surface as a trimer containing three subunits, each

Received: December 21, 2021

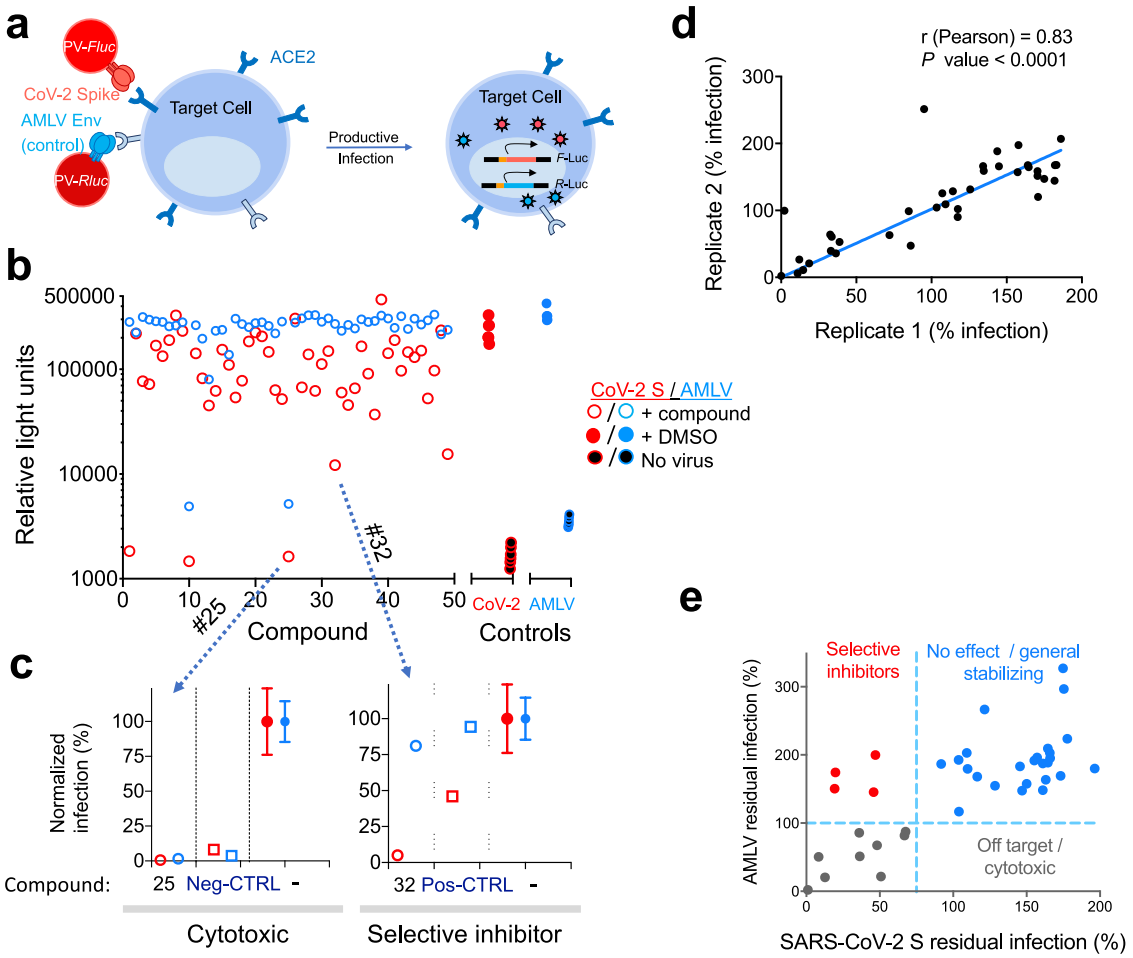

Figure 1. Identification of specific effectors of SARS-CoV-2 entry using an integrated SARS-CoV-2 and control entry system. (a) HIV-1-based PVs mediate the entry of SARS-CoV-2 (left) and, in parallel, the entry of a control, unrelated AMLV. (b) The effect of 49 compounds on both infections was tested. (c) Normalizing the compound effect to no-compound control for each infection generates a specific profile that distinguishes cytotoxic compounds (#25) from specific inhibitors (#32). Neg/Pos-CTRL, negative, and positive controls. (d, e) Statistical and selectivity analysis of selected compounds. (d) In total, 38 hits were selected from the primary screen and retested. For each compound, % residual infection of SARS-CoV-2 spike-mediated entry was calculated, and replicate 1 was plotted against replicate 2. The two-tail *P* value was calculated by Pearson regression analysis. (e) Plotting the effect of each compound on AMLV entry versus its effect on SARS-CoV-2 entry identifies four phenotypes of selectivity.

composed of a 1261-long amino acid glycoprotein (after cleavage of the 12 amino acid signal peptide) that can adopt an open (up) or closed (down) conformation. The transition from a closed to an open spike conformation is required for ACE2 binding and this conformational state is further stabilized in the SARS-CoV-2 D614G mutant that has become dominant in many geographical regions once introduced. In addition, over the last few months, several variants of SARS-CoV-2 have been emerging with increased fitness and higher transmissibility, and few present some degree of resistance to vaccine-elicited neutralizing antibodies. Repurposing of drugs and compounds with known activity holds the potential to accelerate the search for effective therapy against the highly infectious SARS-CoV-2 virus. Two FDA-approved drugs (camostat and losartan) are being tested in clinical trials as treatments for SARS-CoV-2 infection (NCT04335123).[5] However, because both may block SARS-CoV-2 entry by targeting the human TMPRSS2 protease and the ACE2 receptor, which are cellular proteins, these drugs could potentially have significant adverse effects on different systems of the human body.[6,7] In contrast, inhibitors that target the viral SARS-CoV-2 spike are expected to be highly selective and to exhibit minimal off-target effects. In this context, several small-molecule inhibitors of SARS-CoV-2 entry have been recently identified but their target is still under investigation.

Here, we developed a lentivirus-based entry assay to identify SARS-CoV-2 entry inhibition with an integrated ability to simultaneously measure inhibition specificity. We optimized the system and used it to screen a small library of pharmacologically active compounds (LOPAC). We identified selective and broad inhibitors of SARS-CoV-2 entry that share a common core structure. We assessed the breadth of these inhibitors against CoVs and against circulating SARS-CoV-2 variants, investigated their target step of replication, and studied the mode by which these inhibitors block viral entry.

RESULTS

SARS-CoV-2 Entry Assay with an Integrated Control to Measure Compound Specificity can Identify Selective Entry Inhibitors. Based on published data, our previous work, and available reagents, we developed a pseudovirus (PV) assay to study SARS-CoV-2 entry and to identify new small

https://doi.org/10.1021/acsinfecdis.1c00658
ACS Infect. Dis. XXXX, XXX, XXX−XXX

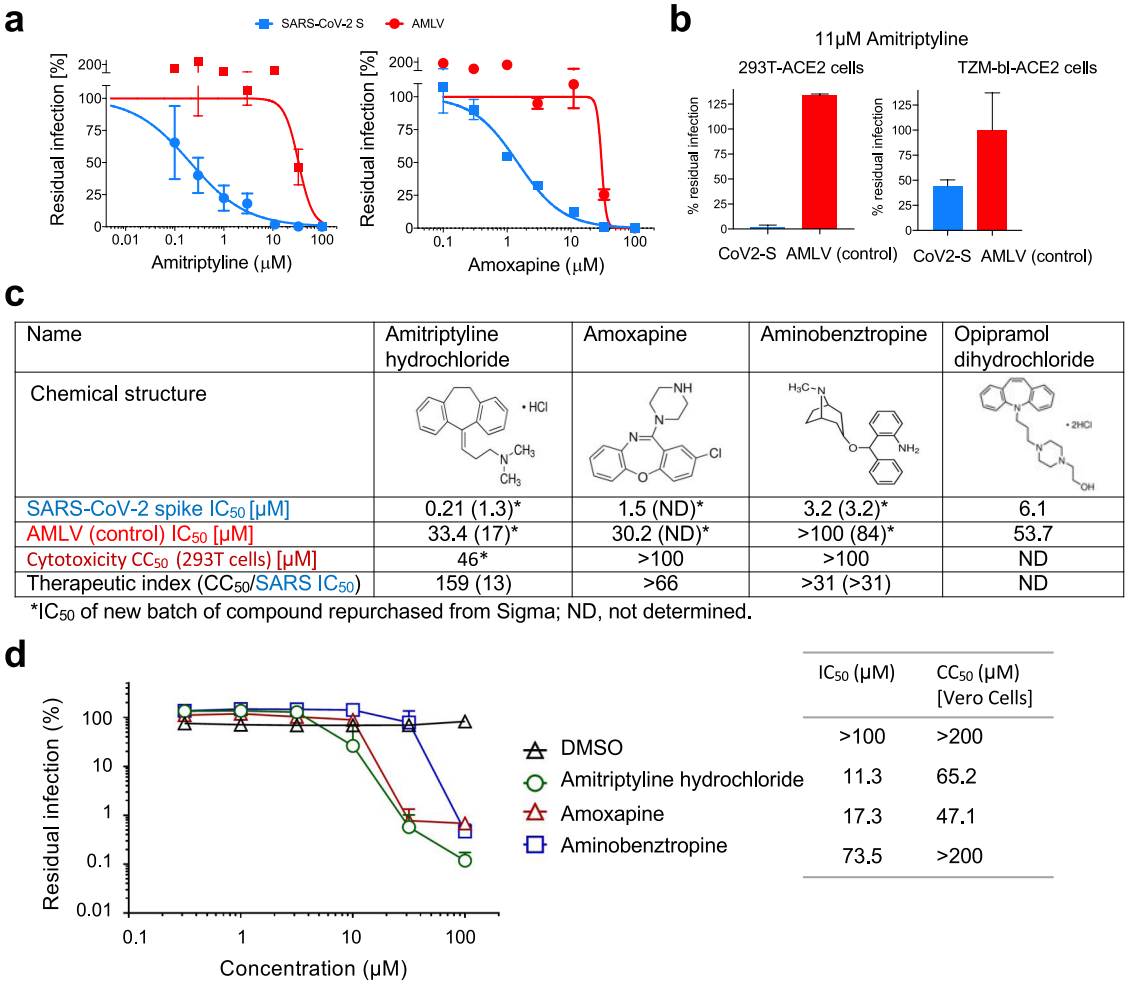

Figure 2. Sensitivity of SARS-CoV-2 entry to three confirmed inhibitors that were identified in the preliminary LOPAC library screen. (a) Increasing concentrations of the compounds (amitriptyline and amoxapine) were tested separately for their effect on SARS-CoV-2 entry or AMLV control entry into 293T-ACE2 cells. (b) Amitriptyline sensitivity of SARS-CoV-2 and AMLV control entry to different target cells that overexpress the ACE2 receptor. (c) Summary of inhibitors' chemical structures and functions. Cytotoxicity was measured using CellTiter-Glo (Promega) under identical experimental conditions. Values in parenthesis denote IC_{50} or CC_{50} or the therapeutic index of a new batch of compounds repurchased from Sigma. (d) Left: sensitivity of replication-competent SARS-CoV-2 to tricyclic entry inhibitors. Right: half-maximal inhibitory and cytotoxic values (IC_{50} and CC_{50}) of compound inhibition.

molecules that either inhibit or enhance viral infection.[8−15] We used an HIV-1-based PV system because this system is well established, stable, and efficient (Figure S1). PVs are prepared by transfecting 293T cells with three plasmids that separately provide: (1) HIV structural proteins and enzymes, (2) HIV genomic RNA containing the *firefly luciferase* (*fluc*) reporter gene to be packed in the budding virus particles, and (3) a virus-specific spike (or envelope glycoproteins). Cells containing the three plasmids produce PVs that display the specific spike on their surface and carry the *fluc* reporter gene. We tested the viral entry mediated by different SARS-CoV spikes into 293T cells overexpressing the human ACE2 receptor (293T-ACE2, provided by Fang Li) and used the parental 293T cells to monitor for background (Figure S1). All four SARS-CoV spikes mediated efficient entry into 293T-ACE2 cells with 100−1000-fold higher efficiency than the entry to the control 293T cells (Figure S1). The SARS-CoV-2 spike mediated less efficient entry than the SARS-CoV-1 spike, but entry efficiency was increased to comparable levels of the SARS-CoV-1 spike when the endocytosis signal was altered and when the carboxyl-terminal 18 amino acids were deleted from the SARS-CoV-2 spike (SARS-CoV-2-Sdel18). Similar results have been reported by several other groups, and the SARS-CoV-2-S with 18−22-residue deletion spike is routinely used by us and others in standard assays (either wild type or the dominant D614G mutant).[16−19] We next tested different conditions and optimized the system (Figure S1c).

Our cell-based system reports a gain of the luciferase enzymatic activity upon productive entry into target cells. Thus, inhibition of entry will decrease luciferase expression, and specific entry inhibitors will reduce assay readout. However, because cytotoxic compounds mimic true positives by simply killing the cells and decreasing the readout, they will mistakenly be scored as positive hits (false positive inhibitors). To limit the false positives rate and to reliably identify specific inhibitors or enhancers, we built a sensitive control assay that measures the entry of the unrelated amphotropic murine leukemia virus (AMLV) to the same target cells but uses *renilla luciferase* (*rluc*) instead of *fluc* as a reporter gene (Figure S2). Engineering a different reporter protein (Rluc) in the AMLV control assay allows us to simultaneously use both viruses: SARS-CoV-2 S (Fluc) and AMLV control (Rluc) in a single

https://doi.org/10.1021/acsinfecdis.1c00658
ACS Infect. Dis. XXXX, XXX, XXX−XXX

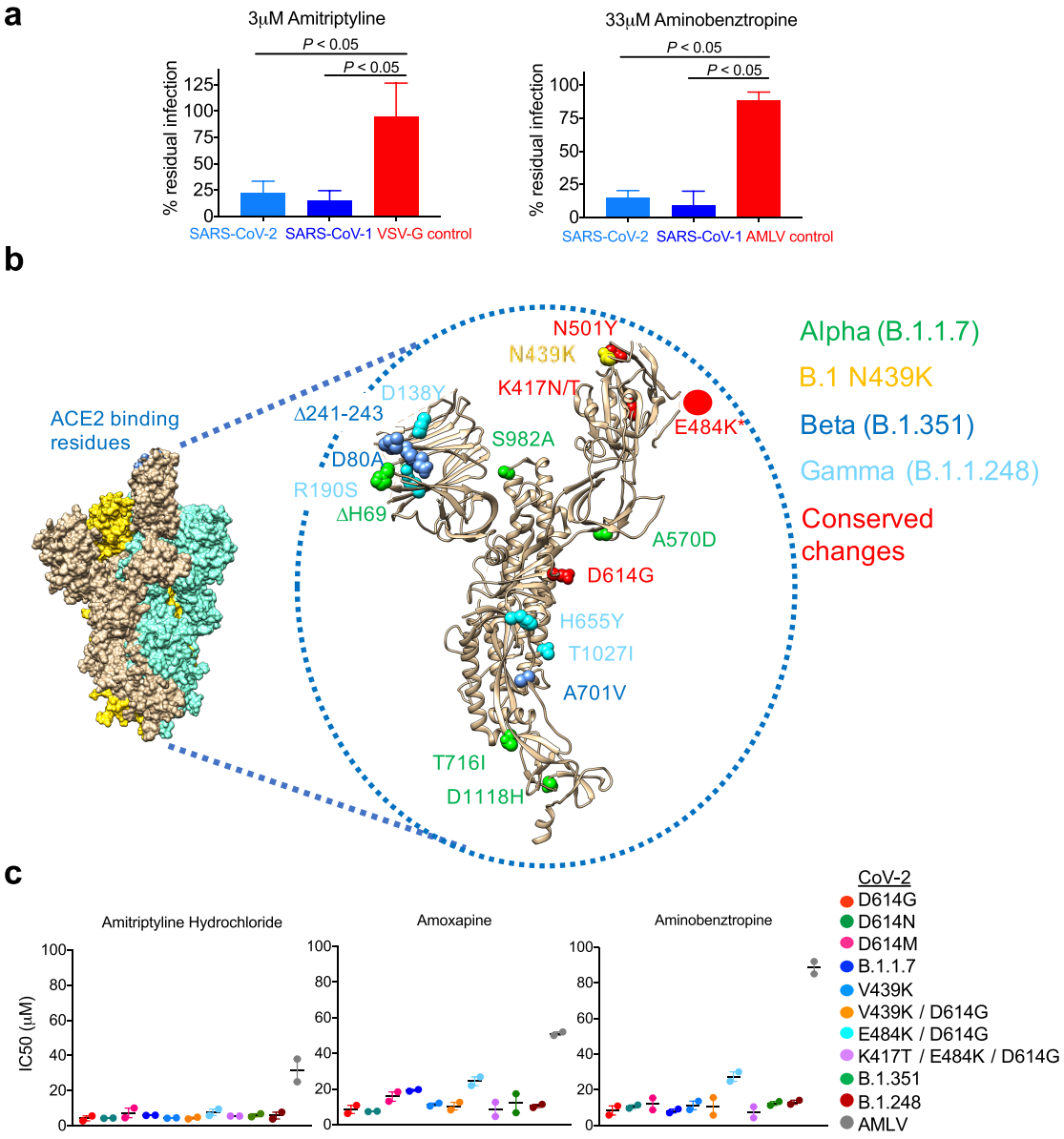

Figure 3. Sensitivity of different SARS-CoVs and SARS-CoV-2 variants to tricyclic entry inhibitors. (a) We tested the sensitivity of PVs displaying SARS-CoV-1 or SARS-CoV-2 spikes to amitriptyline (left) or aminobenztropine (right). VSV-G or AMLV was used as control. One-tail *t*-test was used to calculate statistical significance (*P* value). (b) Main amino acid changes in circulating SARS-CoV-2 spike variants were mapped on the available cryo-EM prefusion structure of the soluble SARS-CoV-2 spike (protein database entry 6VSB). Not all changes are shown; * an estimated position of residue 484 is schematically shown. (c) Sensitivity of SARS-CoV-2 variants circulating in the viral population to tricyclic ring entry inhibitors.

well, infecting exactly the same cells and incubating with exactly the same test compound [in this system, all pseudoviral components were identical except for (a) the envelope glycoproteins/spike and (b) the reporter protein; subsequent experiments confirmed specific entry inhibition by comparing side-by-side pseudoviruses that carry the *fluc* reporter gene and display the SARS-CoV-2 spike with identical fluc pseudoviruses that display AMLV/VSV-G envelope glycoproteins/spike]. The activity of the two luciferases can be separately detected using their related, different substrates.[11] This approach significantly reduces the cost, time, and labor of running a control assay in parallel to the main SARS-CoV-2 entry assay and ensures identical experimental conditions (medium, cells, and compound). We tested the effect of 49 compounds from the LOPAC library on our integrated system. Both assays were highly reproducible and robust with signal-to-noise ratios of 141 (SARS-CoV-2 entry) and 93 (AMLV entry) and low variation among the readouts from wells with similar assay conditions. The analysis of the raw data showed significant differences in the profile of several compounds (e.g., compound 25 vs 32; dashed arrows in Figure 1b,c). To compare the effect of compounds on SARS-CoV-2 entry with their effect on AMLV control entry, we normalized the readout of each compound to no-compound control for each infection (Figure 1c). The normalized readout of both assays generated a specific profile for each compound that allowed us to distinguish specific inhibitors, like soluble ACE2 (positive control), from cytotoxic compounds like high doses of chloroquine (negative control; Figure 1c). More importantly, we could readily identify selective inhibitors (#32) and

https://doi.org/10.1021/acsinfecdis.1c00658
ACS Infect. Dis. XXXX, XXX, XXX−XXX

eliminate cytotoxic compounds (#25; Figure 1c). We therefore used in subsequent experiments the readout of AMLV-mediated entry as specificity control, either in one integrated system (using Fluc and Rluc activities in parallel) or by measuring separately the effects of compounds on SARS-CoV-2 spike-mediated entry and the effects of the same compounds on AMLV-mediated entry.

Tricyclic Compounds Selectively Block SARS-CoV-2 Entry. To test the performance of our viral entry system, we screened 551 compounds from a small library of pharmacologically active compounds (LOPAC; available from Sigma), for effectors of SARS-CoV-2 entry. The LOPAC library contains approved drugs, candidate drugs developed to different stages, and compounds with well-characterized activities. Measurements were robust and reproducible with a highly significant correlation between the replicates (Figure 1d). We analyzed the selectivity of each compound by plotting % residual infection of AMLV control against % residual infection of SARS-CoV-2, both in the presence of a test compound, and identified four selective inhibitors of SARS-CoV-2 entry: amitriptyline, amoxapine, aminobenztropine, and opipramol (Figure 2). We confirmed selective SARS-CoV-2 inhibition by testing compounds from different batches, using a viral assay with the same fluc reporter protein (for SARS-CoV-2 spike and AMLV), and testing different cell types that overexpress the ACE2 receptor (Figure 2). All four compounds shared functional chemical groups, with three compounds sharing a tricyclic ring system, and the fourth (aminobenztropine) containing two aromatic rings that are separated by a flexible methyl group that adopts a spatial structure similar to a tricyclic ring system (Figure 2c). We further refer to this group of compounds as tricyclic inhibitors, although aminobenztropine does not contain a tricyclic ring system. Since opipramol has been already identified and described in a published study,[20] we focused in most of our subsequent work on the other three inhibitors. All three compounds (amitriptyline, amoxapine, and aminobenztropine) inhibited live SARS-CoV-2 replication with a similar inhibition pattern as inhibition of the SARS-Cov-2 spike pseudoviruses but they were about 1 order of magnitude less potent under the experimental conditions tested during replication-competent infection of Vero cells (Figure 2d).

Tricyclic Inhibitors Block the Entry of Different SARS-CoVs and Circulating Variants. The development of SARS-CoV-2 variants that are resistant to current vaccines and/or exhibit increased fitness and replication capacity is a major public health concern. Moreover, the emergence of SARS-CoV-1, Middle East respiratory syndrome (MERS)-CoV, and SARS-CoV-2 within the last 20 years highlights a need for broad-range entry inhibitors that would potentially be effective against emerging CoVs in the future. Therefore, we evaluated the breadth of our tricyclic entry inhibitors against different CoVs and circulating variants (Figure 3). Both amitriptyline and aminobenztropine inhibited SARS-CoV-1 and SARS-CoV-2 to comparable levels with approximately 80% reduction in viral entry at 3 and 33 μM, respectively. In contrast, the entry mediated by the controls VSV-G and AMLV Env was not significantly affected, suggesting that these inhibitors are broad and highly selective. We next measured the sensitivity of a large panel of SARS-CoV-2 variants that have evolved to replicate in the human population and are currently circulating in the viral population to our inhibitors. Two spreading variants, B.1.351 and B.1.1.248, which were initially identified in South Africa and Brazil, respectively, exhibited decreased sensitivity to antibodies elicited by the wild-type vaccines and led to efforts to modify current vaccine immunogens. B.1.351 and B.1.1.248 share amino acid changes in four core residues: N417, E484, N501, and D614. We, therefore, generated SARS-CoV-2 spike mutants with changes only in these residues (Figure 3). The V439K SARS-CoV-2 variant is relatively resistant to antibodies developed on convalescent serum. Consistent with their ability to block SARS-CoV-1 and SARS-CoV-2 entry, the broad tricyclic entry inhibitors effectively blocked the entry of all SARS-CoV-2 variants tested. These included the B.1.351 and B.1.1.248 variants as well as the dominant D614G variant and variants carrying changes in residue 614 to Asn or Met amino acids. The most selective compound was aminobenztropine that efficiently blocked all SARS-CoV-2 spike variants and had no or very minimal effects on the AMLV control-mediated infection. Of note, the E484K + D614G variant was less sensitive to amoxapine and aminobeztropine than other variants but additional changes in B.1.351 and B.1.1.248 restored wild-type (D614G) sensitivity.

We next studied the viral step that these compounds are targeting by investigating the effect of aminobenztropine addition at different time points post infection. We focused on aminobenztropine because the compound exhibits no or very minimal no-specific effects on the AMLV control-mediated infection (Figure 2c). We detected a gradual decrease in entry inhibition for SARS-CoV-2 spike-mediated infection when aminobenztropine was added at later time points with no significant effects when the compound was added after overnight incubation (Figure 4). As expected, we

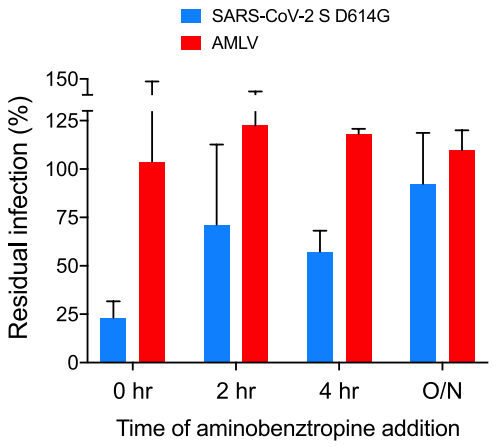

Figure 4. Time of inhibitor activity. Aminobenztropine (25 μM) was added at specified time points during SARS-CoV-2 spike or AMLV control-mediated infection. Residual infection was measured after 72 h and normalized to dimethyl sulfoxide (DMSO)-only control. O/N, overnight.

did not detect any significant effect on AMLV control-mediated infection. These results further indicate that aminobenztropine is blocking an early step in the virus replication cycle. As our identified inhibitors block different neurotransmitters at synapses in the central and peripheral nervous system and contain a common tricyclic (or similar) ring system, we identified additional drugs with similar properties and tested their inhibition activity (Table S1). All compounds exhibited selective inhibition of SARS-CoV-2 spike-mediated entry compared to AMLV control-mediated entry with diverse degrees of potency and selectivity, further

https://doi.org/10.1021/acsinfecdis.1c00658
ACS Infect. Dis. XXXX, XXX, XXX−XXX

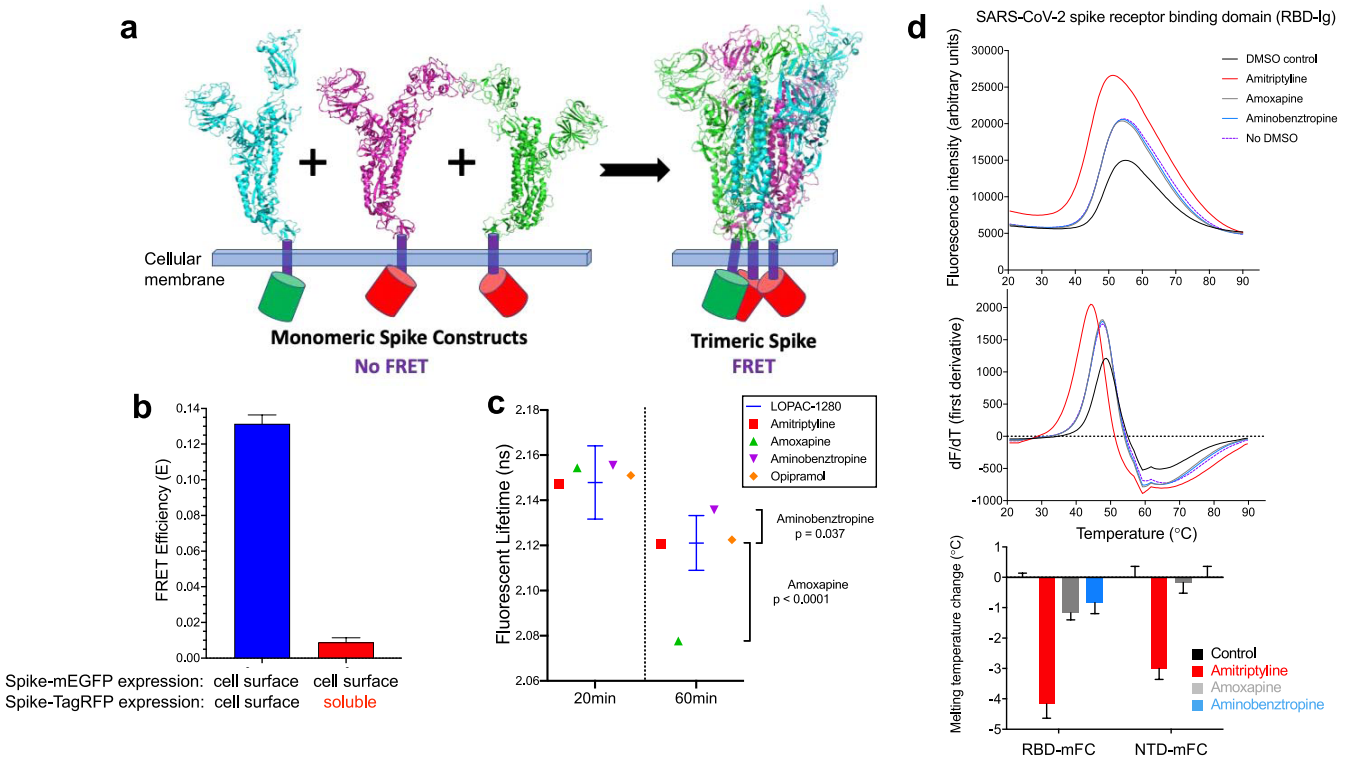

Figure 5. SARS-CoV-2 spike−small molecule interactions. (a) Our cellular FLT-FRET biosensor comprises a monomeric, full-length SARS-CoV-2-spike glycoprotein fused to either donor (mEGFP) or acceptor (TagRFP-T) fluorescent proteins. Transient coexpression of both donor and acceptor constructs in HEK293 cells results in spike oligomerization and increases the FRET readout (measured as fluorescence lifetime). We optimized the signal-to-noise ratio by altering donor and acceptor expression levels. The ribbon-displayed spike structure was adapted from the research collaboratory for structural bioinformatics (RCSB) database (protein data entry 6crz).[26] (b) Our FLT-FRET signal is specific to the SARS-CoV-2 spike glycoprotein, as coexpression of spike-mEGFP and soluble TagRFP results in minimal basal FRET. (c) The interaction of the CoV-2 spike with our four inhibitors at 10 μM was tested by FLT-FRET and compared to the average FLT response of 1280 compounds from the LOPAC library. Two-tail *t*-test was used to calculate the statistical significance (*P* value) of FLT changes. (d) Thermal shift analysis of the soluble receptor binding domain (RBD) and the N-terminal domain (NTD) of the SARS-CoV-2 spike fused to the monomeric FC region of IgG (mFC). Top panel: average raw data of the RBD shift in the presence and absence of indicated compounds. Middle panel: similar to the top panel but the first derivative (d fluorescence/d temperature; d F/d T) is plotted against temperature. Bottom panel: thermal shifts of melting temperatures in each condition. n = 3; mean and standard error of mean (SEM) are shown. Compounds were tested at 1 mM (amitriptyline) or 0.25 mM (amoxapine and aminobenztropine) concentrations.

supporting the role of tricyclic ring systems in selective inhibition activity of SARS-CoV-2 entry.

Interactions between SARS-CoV-2 Spike and Tricyclic Inhibitors. We developed a live-cell fluorescence lifetime (FLT) assay based on a fluorescence resonance energy transfer (FRET) biosensor to monitor SARS-CoV-2 spike assembly and conformational changes (Figure 5a). FLT-FRET technology is 30-fold more precise than steady-state intensity FRET assays, improving our assay's coefficient of variation (CV) and decreasing the probability of false negatives.[21−25] The FLT change is specific to spike−spike interactions as cotransfection of full-length spike-mEGFP (donor) and soluble TagRFP (acceptor) results in a low background FRET signal (Figure 5b) relative to the FLT of our biosensor expressing full-length spike-mEGFP (donor) and full-length spike-TagRFP (acceptor).

We compared the SARS-CoV-2 spike FLT-FRET response of our tricyclic inhibitors to the response of 1280 compounds from the LOPAC library and identified two inhibitors that significantly altered the FLT-FRET readout after 60 min incubation (Figure 5c). Aminobenztropine increased the FLT (decreased FRET, corresponding to increased distances between donor and acceptor fusion proteins) response, whereas amoxapine had the opposite effect and substantially decreased the FLT response (increased FRET, suggesting increased assembly or change in assembled trimer conformation). To gain additional insights into the binding target of our tricyclic entry inhibitors to the SARS-CoV-2 spike, we measured the effects of each compound on the thermal shifts of different regions of the SARS-CoV-2 spike. Both amoxapine and aminobenztropine selectively altered the melting temperature (T_m) of the receptor binding domain (RBD) of the SARS-CoV-2 spike without significant effects on the T_m of the N-terminal domain (NTD) of the viral spike. Amitriptyline decreased the T_m of both RBD and NTD, probably due to nonspecific interaction with the IgG FC domains that are fused to each, but the effects on RBD were still more profound. To measure direct interactions of the compounds with the SARS-CoV-2 spike, we selected two compounds, aminobenztropine and opipramol, and monitored their direct binding kinetics and equilibrium to the spike using surface plasmon resonance technology (SPR; by BIAcore S200). Both compounds interacted directly with the SARS-CoV-2 spike according to the SPR response, and the magnitude of the response was dose-dependent (Figure 6). We noted that the maximum response (R_{max}) was higher than the predicted theoretical R_{max},

https://doi.org/10.1021/acsinfecdis.1c00658
ACS Infect. Dis. XXXX, XXX, XXX−XXX

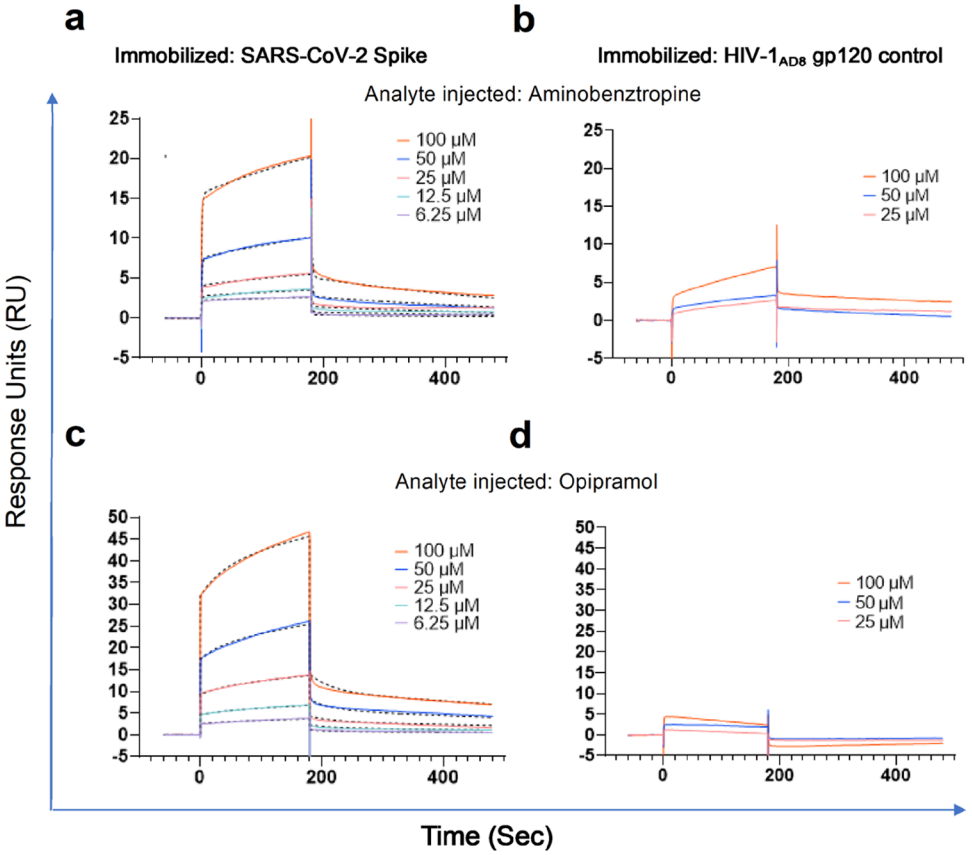

Figure 6. SARS-CoV-2 spike−small molecule direct interactions. SPR curves (sensorgrams) of binding of aminobenztropine and opipramol to the soluble SARS-CoV-2 spike glycoprotein (ectodomain) or to soluble HIV-1_{AD8} gp120 control. SPR experiments were performed on a Biacore S200 instrument. Two-fold serial dilutions of aminobenztropine or opipramol dissolved in running buffer (PBS-P+, 1% DMSO) were injected across SARS-CoV-2 spike (a, c) or HIV_{AD8}-gp120 (b, d) glycoproteins that were immobilized through the 8-histidine tag on an NTA series S sensor chip. The data (sensorgrams) from SARS-CoV-2 spike binding to the two compounds (solid lines) were nonlinearly fitted to a two-state binding model (dashed lines).

which suggests some nonspecific binding or complex interactions of the cyclic aromatic rings with the SPR sensor surface, and therefore, we tested the binding of these compounds to an unrelated soluble viral envelope glycoprotein (gp120) of HIV-1 as a control. Binding to the control gp120 was minimal and only at the highest concentration, confirming specific interactions of the compounds with the SARS-CoV-2 spike. We did not test the potential binding of the compounds to the ACE2 receptor. Together, these observations suggest that the compounds bind to a specific pocket located in the RBD of the SARS-CoV-2 spike, with amoxapine and aminobenztropine inducing different changes in the spike conformation/assembly.

To study the mechanism of inhibition, we investigated the effects of the tricyclic ring inhibitors on the ability of the SARS-CoV-2 spike to mediate cell−cell fusion activity. The tricyclic inhibitors efficiently blocked cell−cell fusion but exhibited lower potency than the one observed for viral entry inhibition (Figure 7). As the number of SARS-CoV-2 spikes on the cell surface is significantly higher than the number of spikes on viral particles, this pattern reflects the requirement to block highly efficient cell−cell fusing events that can occur in numerous sites of interactions. We next assessed the interference of our inhibitors with interactions of the SARS-CoV-2 spike with different ligands by flow cytometry using the cell-surface-expressed SASR-CoV-2 spike and soluble ligands. Notably, we did not detect any significant effects of tricyclic ring inhibitors on the binding of the SARS-CoV-2 spike to the soluble ACE2 receptor or to the specific CC6.33 monoclonal antibody, which recognizes the ACE2 binding site on the viral spike (Figure 7). Even at a very high inhibitor concentration of 300 μM, which was not cytotoxic to the cells during the short exposure time of the assay, and at very low ligand concentrations, no significant difference was observed between the compounds and DMSO control. Similar results were detected for the binding of the SARS-CoV-1 spike to the soluble ACE2 receptor.

DISCUSSION

SARS-CoV-2 entry into host cells is mediated by specific interactions of the viral, envelope-anchored spike glycoprotein with the host ACE2 receptor.[6,27] SARS-CoV-2 spike binding to ACE2 initiates viral infection and, thus, compounds that disrupt this recognition or prevent subsequent step(s) critical for entry could be therapeutically useful and instrumental for understanding the biology of SARS-CoV-2 entry.[28−34] To identify such compounds, we built an integrated SARS-CoV-2 entry assay that is based on a lentiviral system and contains a built-in control for evaluating the specificity of each compound.[35] Comparing the effects of test compounds on the entry of SARS-CoV-2 with their effects on the entry of unrelated AMLV control allowed us to identify selective tricyclic ring inhibitors of SARS-CoV-2 entry.[36] Our study

https://doi.org/10.1021/acsinfecdis.1c00658
ACS Infect. Dis. XXXX, XXX, XXX−XXX

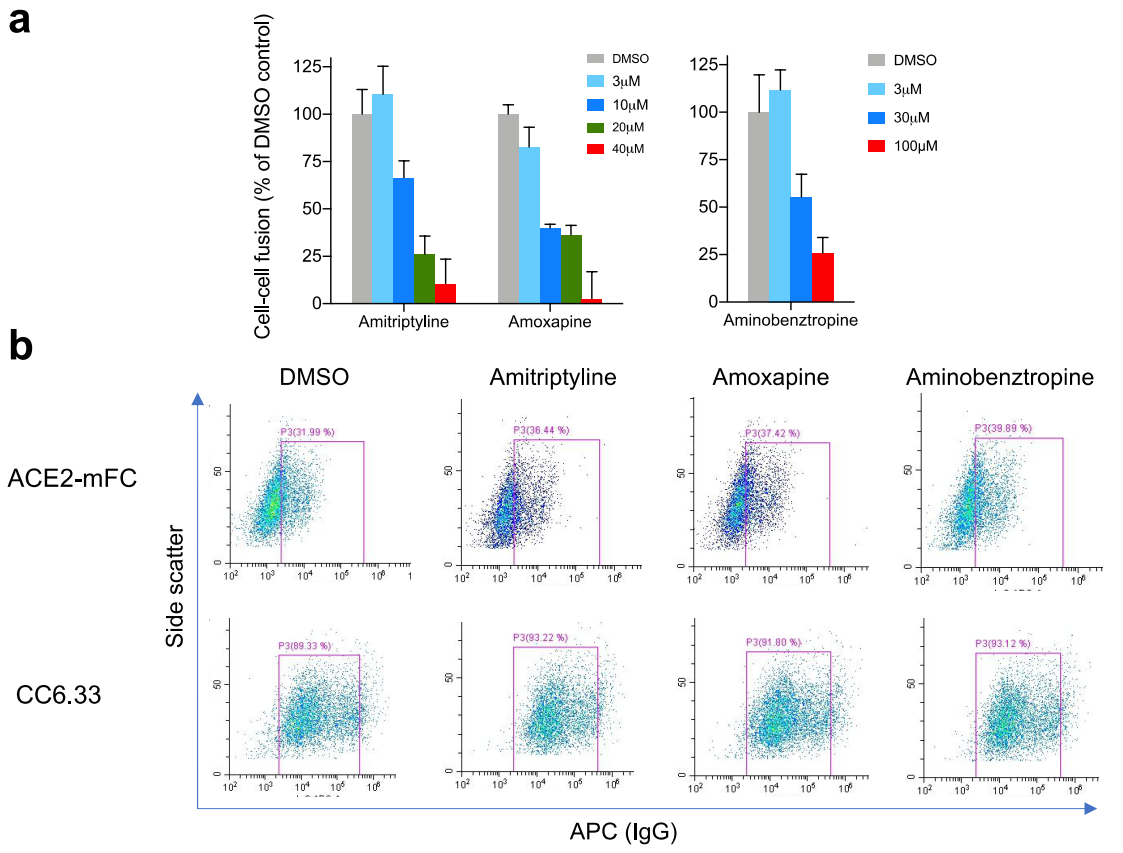

Figure 7. Tricyclic entry inhibitors block spike-mediated cell−cell fusion activity without interfering with SARS-CoV spike−ACE2 interactions. (a) Effects of tricyclic inhibitors on SARS-CoV-2 spike-mediated cell−cell fusion. We measured the fusion of effector cells expressing the SARS-CoV-2 spike and HIV-1 Tat that were cocultured with 293T-ACE2 target cells transfected with a reporter plasmid. Fusion of these cells leads to the transport of HIV-1 Tat to the 293T-ACE2 target cells and activation of firefly luciferase expression. (b) Flow cytometric analysis of the effects of entry inhibitors on the binding of the cell-surface-expressed SARS-CoV-2 spike to soluble ACE2-mFC and to the CC6.33 antibody.

identified four compounds, three of which, amitriptyline, amoxapine, and opipramol dihydrochloride, are FDA-approved tricyclic antidepressant (TCA) drugs and are commonly used to treat anxiety and depression. The antidepressant effects of these drugs require much lower concentrations than those observed in our study for blocking SASR-CoV-2 entry. Thus, these compounds, which were identified as initial hits in a small screen, will need extensive optimization and significant improvement of their selectivity for any potential future application as drugs or chemical probes. Limited studies have demonstrated that fluvoxamine, which is an antidepressant that does not contain a tricyclic ring system and could offer mild protection against the coronaviruses, prevents clinical deterioration, and helps fight the early infection phase,[37,38] though no concrete clinical data are available to date. Notably, we found that several additional tricyclic antidepressant compounds exhibited selective entry inhibition of SARS-CoV-2 (Table S1). Of note, other tricyclic compounds tested, including closely related analogues such as imipramine and trimipramine, were significantly less potent SARS-CoV-2 entry inhibitors than amitriptyline. In parallel, several additional and independent studies have reported selective SASR-CoV-2 entry inhibition by different tricyclic antidepressant drugs using different experimental systems and different target cells (methylene blue, clomipramine, trimipramine, trimeprazine, flupenthixol, clofazimine; see Table S2).[39−43] These include inhibition of SARS-CoV-2 infection by opipramol dihydrochloride in Vero E6 and Caco2 cells, inhibition of SARS-CoV-2 spike-mediated cell−cell fusion by clofazimine, and inhibition of SARS-CoV-2 replication in a hamster model by clofazimine.[20,44,45]

Our compounds, similar to other SARS-CoV-2 entry inhibitors identified in previous studies, belong to a group of cationic amphiphilic drugs (CADs). Despite their in vitro potential side effects, which may include phospholipidosis,[46] they are directly interacting with their targets and have been used in patients for years. Amitriptyline, amoxapine, and opipramol dihydrochloride are FDA-approved tricyclic antidepressants. We have shown by multiple different assays, including SPR (BIAcore; Figure 6), the direct interactions of our inhibitors with the SARS-CoV-2 spike; we also showed specific inhibition of SARS-CoV-2 spike-mediated entry compared to AMLV- or VSV-G-mediated entry, confirming that despite any potential side effect on the target cells, including phospholipidosis, the compounds selectively block SARS-CoV-2 entry more efficiently than the entry of other viruses. The identification of different compounds with common tricyclic groups by us and other groups further support the specificity of the inhibition. Thus, we believe that the tricyclic group provides an important guide and a useful scaffold for building a pharmacophore for the development of broad entry inhibitors of CoVs. Importantly, our study highlights the potential of such compounds to block the

https://doi.org/10.1021/acsinfecdis.1c00658
ACS Infect. Dis. XXXX, XXX, XXX−XXX

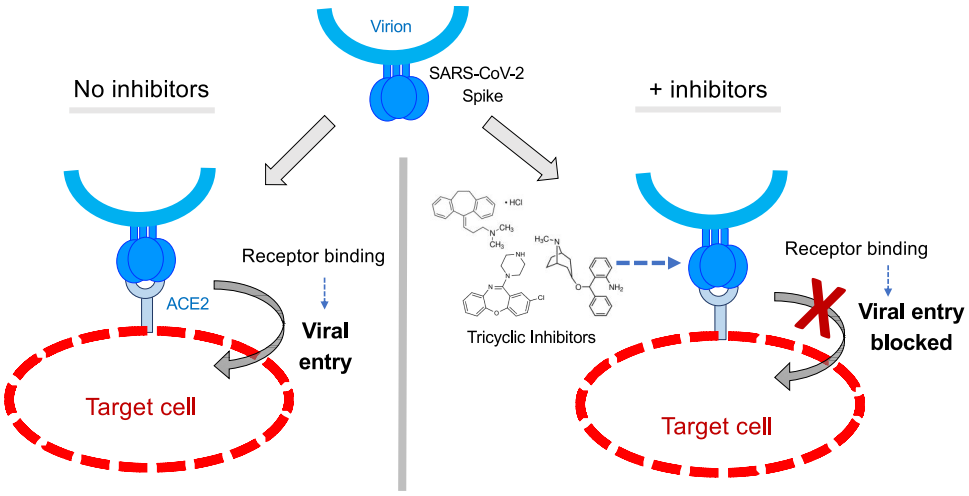

Figure 8. Proposed model of SARS-CoV entry inhibition by tricyclic inhibitors. SARS-CoV-2 spike binds to the ACE2 receptor and mediates viral entry (left). In the presence of tricyclic ring inhibitors, the viral spike can still bind the cellular receptor but subsequent steps on the entry pathway are blocked (right).

entry of SARS-CoV-1, SARS-CoV-2, and many SARS-CoV-2 variants that have recently emerged.

Combing different biochemical, biophysical, and immunological approaches allowed us to provide important insights into the mechanisms of SARS-CoV-2 entry inhibition by tricyclic inhibitors. Our FRET-based assay to monitor the effect of small molecules on the CoV-2 spike integrity and thermal shift analysis indicate that tricyclic entry inhibitors can directly interact with the SARS-CoV-2 spike and induce different changes in spike conformation/assembly. However, these compounds do not interfere with the binding of the ACE2 receptor or the CC6.33 antibody, which is specific for the receptor binding site on SARS-CoV spikes. Altogether, these data support a model in which tricycle ring inhibitors bind to a highly conserved site that is not involved in ACE2 binding and block viral activity or transitions that are required for moving forward on the entry pathway and/or mediating cell−cell fusion activity (Figure 8). Notably, we identified a similar mode of inhibition with a specific group of inhibitors that block conformational transitions of HIV-1 envelope glycoproteins (Envs) and include 484, 18A, and the FDA-approved drug BMS-626529 (fostemsavir). As these compounds block conformational transitions and stabilize the prefusion conformation of HIV-1 Envs, they are routinely used to study the biology of HIV-1 entry and can be further developed for treatment and prevention strategies. The effect of tricyclic inhibitors on SARS- CoV-2 spike conformation is still under investigation. Nevertheless, since most of these compounds also interfere with neurotransmitter retake by different receptors that belong to the nervous system, we hypothesize that the SARS-CoV-2 spike contains a binding pocket that fits compounds containing tricyclic rings and may share common elements with the binding site of these cellular receptors. Furthermore, common features may be shared with similar pockets on other viral envelope glycoproteins as benztropine (a derivative of aminobenztropine) directly binds to the Ebola envelope glycoprotein and blocks viral entry.[47] Taken together, our results provide new insights into SARS-CoV-2 spikes, possibilities to use these small molecules to map the pathway of SARS-CoV-2 entry, and means to target virus entry.

METHODS

Cell Lines. 293T cells were purchased from ATCC. TZM-bl cells were obtained from the NIH AIDS Reagent Program. 293T cells overexpressing the human ACE2 receptor (293T-ACE2) were a kind gift from Fang Li, the University of Minnesota; TZM-bl-ACE2 cells were a kind gift from Michael Farzan, Scripps Florida. Both cell lines were grown in Dulbecco's modified Eagle medium (DMEM) containing 10% fetal bovine serum (FBS), 100 μg/mL streptomycin, and 100 U/mL penicillin at 37 °C with 5% CO_2. ACE2 expression was maintained by supplementing the medium with 3 μg/mL (293T-ACE2 cells) or 1 μg/mL (TZM-bl-ACE2 cells) of the selection antibiotic puromycin. All cells were tested periodically for mycoplasma contamination.

Plasmid Construction. Plasmid expressing a full-length SARS-CoV-2 spike was kindly provided by Stefan Pöhlmann, Leibniz Institute for Primate Research, Göttingen, Germany. SARS-CoV-2 spike mutants were constructed by site-directed mutagenesis or by gene synthesis (Gene Universal), and the correct DNA sequence was verified by Sanger sequencing.

Production of Recombinant SARS-CoVs Expressing Luciferase. We produced viral spike/envelope glycoprotein pseudotyped viruses by cotransfecting 293T cells with three plasmids that separately provide: (1) a virus-specific spike (or envelope glycoproteins), (2) HIV-1-based packaging plasmid, (3) a lentiviral reporter vector containing the *firefly luciferase* (*fluc*) or *renilla luciferase* (*rluc*) genes to be packed in the budding virus particles using Effectene (QIAGEN). After a 48 h incubation, the cell supernatant was collected and centrifuged for 5 min at 600−900*g* at 4 °C. The amount of p24 in the supernatant was measured using an in-house HIV-1 p24 antigen capture assay as previously described.[48] The virus-containing supernatant was frozen in single-use aliquots at −80 °C.

Single-Round (PVs) Viral Infection Assay. We tested the viral entry mediated by different SARS-CoV spikes into 293T-ACE2 target cells and, in most cases, used the parental 293T cells to monitor for background (Figure S1). Different PVs were added to each well of a 96-well plate (Greiner bio-one 96-well plates Cat# 655083), followed by addition of 7200 target cells/well in a final volume of 100 μL. Control wells

https://doi.org/10.1021/acsinfecdis.1c00658
ACS Infect. Dis. XXXX, XXX, XXX−XXX

included PV infection mediated by unrelated Envs (derived from the amphotropic murine leukemia virus (AMLV) or vesicular stomatitis virus (VSV)), infection of 293T cells, which do not express the ACE2 receptor, target 293T-ACE2 cells with no PVs, and PVs with no cells in 100 μL/well. After 48−72 h incubation in a tissue culture incubator at 37 °C and 5% CO_2 concentration, the medium from the wells was aspirated and 30 μL/well lysis buffer was added.[48,49] The activity of firefly luciferase, which was used as a reporter protein in the system, was measured with a Centro XS^3 luminometer (Berthold Technologies, Tennessee), and the results were analyzed as we previously described.[48,49] For integration of test and control assays into one system, AMLV Envs PV carrying the *renilla luciferase* (*rluc*) reporter gene were added together with SARS-CoV-2 spike PVs to 293T-ACE2 target cells, incubated for 48−72 h, and then lysed. Both *fluc* and rluc activities can be measured sequentially from a single sample as we previously described.[11] For experiments involving small molecules, compounds were added to each well followed by the addition of PVs and target cells; DMSO concentration was 1% and the final volume was 100 μL, with control cells containing 1% DMSO without any compound.

SARS-CoV-2 Microneutralization Assay. The sensitivity of live SARS-CoV-2 D614G to compounds was measured as previously described.[50] One day prior to infection, 2×10^4 Vero E6 cells were seeded in each test well of a 96-well flat bottom plate and incubated overnight. Compounds were diluted in a separate 96-well culture plate using DMEM supplemented with penicillin (100 U/mL), streptomycin (100 μg/mL), 4-(2-hydroxyethyl)-1-piperazineethanesulfonic acid (HEPES), 0.12% sodium bicarbonate, 2% FBS, and 0.24% bovine serum albumin (BSA). Next, 10^4 $TCID_{50}$/mL SARS-CoV-2 viruses were prepared in DMEM + 2% FBS and combined with an equivalent volume of diluted compounds for 1 h (final compound concentrations were 0, 0.316, 1, 3.16, 10, 31.6, and 100 μM). After incubation, media was removed from the 96-well plate seeded with Vero E6 cells followed by the addition of the SARS-CoV-2/compound mixture to each respective well at a volume corresponding to 600 $TCID_{50}$ per well, and the plate was incubated for an additional 1 h at 37 °C. Both SARS-CoV-2-only and media-only (DMEM + 2% FBS) controls were included in the assay. The supernatant containing SARS-CoV-2 and the compound was removed from wells without disrupting the Vero E6 monolayer, DMEM + 2% FBS containing the respective diluted compound was added to each well, and the plate was incubated for 48 h. Media in each well was replaced with 10% formaldehyde and incubated for 24 h to cross-link the Vero E6 monolayer. The formaldehyde solution was then removed from the wells, and the wells were subsequently washed with PBS. Cell monolayers were permeabilized for 15 min at room temperature with PBS + 0.1% Triton X-100, washed with PBS, and then incubated for 1 h at room temperature with PBS + 3% nonfat milk. A 1 μg/mL anti-mouse SARS-CoV-2 nucleocapsid protein (Clone 1C7, Bioss Antibodies) primary antibody solution in PBS + 1% nonfat milk was added to all wells, and the plate was incubated for 1 h at room temperature. The wells were extensively washed three times with PBS and incubated with the anti-mouse IgG HRP secondary antibody (1:2500 dilution) in PBS + 1% nonfat milk. Then, 1 h post-room temperature incubation, the wells were washed three times with PBS, an enhanced chemiluminescent substrate (Western Lightning Plus-ECL, PerkinElmer) was added, and the readout in each well was measured using an LB941 TriStar luminometer (Berthold Technologies).

Screening of a Library of Pharmacologically Active Compounds. We screened a small library of pharmacologically active compounds (LOPAC; available from Sigma), to find potential inhibitors of SARS-CoV-2 entry using our integrated dual luciferase reporter assay system in a 96-well format in cell-culture plates. Besides, pharmacologically active compounds with well-characterized functions, the LOPAC library also includes licensed and marketed drugs. We also tested the effects of inhibitors (soluble ACE2 and chloroquine) at variable concentrations on SARS-CoV-2 entry. Initially, we prepared the plates with different LOPAC molecules at a final concentration of 10 μM (2% DMSO) of inhibitors in duplicates, followed by incubation with PVs displaying specific SARS-CoV-2 envelopes and AMLV control for 1 h at 37 °C. We normally use specific p24 amounts in the range of 1−10 ng or infectivity values equivalent to approximately 1 million relative light units. Since compounds were dissolved in DMSO, we used identical concentration of 2% DMSO as a reference to account for the DMSO effect. 293T-ACE2 target cells resuspended in DMEM (2.4×10^5 cells/mL) were added and incubated for 48/72 h at 37 °C with 5% CO_2. *Fluc* and *rluc* reporter expression was determined sequentially as mentioned in the previous section.

Dose−Response Curves. Compounds identified in our preliminary screening of the LOPAC library as selective inhibitors of SARS-CoV-2 entry were tested for dose response. We tested the increasing concentrations of the selected compounds starting from 0.01 μM to as high as 100 μM. Compounds were serially diluted in DMSO and added to the wells in duplicates/triplicates, followed by the addition of reporter viruses (or a mixture of two reporter viruses) and then target cells (293T-ACE2/TZM-bl-ACE2, 2.4×10^5 cells/mL), keeping the total volume in a single well to 100 μL. Plates were incubated for 48/72 h at 37 °C and 5% CO_2, and luciferase expression was determined in the same manner as done previously.

FRET Assay. *SARS-CoV-2-Spike−Inhibitor Interactions.* We developed a live-cell fluorescence lifetime (FLT) assay based on a fluorescence resonance energy transfer (FRET) biosensor to monitor SARS-CoV-2 spike assembly and conformational changes. The full-length SARS-CoV-2 spike gene was separately cloned into two plasmids to generate a biosensor system comprising spike-mEGFP (donor) and spike-TagRFP (acceptor) expression plasmids. The resulting plasmids were transiently transfected (lipofectamine 3000, Thermo Fisher) into 293T cells. The FLT-FRET assay was performed 48 h post transfection following established lab protocols.[22,25,51,52] The cells were harvested by incubating with TrypLE (Invitrogen) for 5 min, washed three times in PBS by centrifugation at 200*g*, and filtered using 70 μm cell strainers (BD Falcon). Cell viability was assessed prior to the FLT assay using a trypan blue assay to ensure that the viability was >90%. The cells were then diluted to 1e6 cells/mL using an automated cell counter (CellDrop, DeNovix) and plated (5 μL/well) using a Multidrop Combi Reagent Dispenser (Thermo Fisher Scientific) into 1536-well assay plates containing the compounds or DMSO control. The plates were sealed and allowed to incubate at room temperature for 20 and 60 min prior to FLT measurements. FLT was measured using our FLT-plate reader with a 473 nm pulsed laser and FRET determined by FRET = $1 - \tau_{DA}/\tau_D$, using donor-only

https://doi.org/10.1021/acsinfecdis.1c00658
ACS Infect. Dis. XXXX, XXX, XXX−XXX

(D) and donor-acceptor (DA) FLT measurements.[21,53] We compared the SARS-CoV-2 spike FLT-FRET response of the selected inhibitors (10 μM) to the average response of the 1280 compounds of the LOPAC library.

Data Analysis. To identify selective SARS-CoV-2 entry inhibitors, we set the selection criteria to (1) % activity < 50 (compounds that decrease SARS-CoV-2-mediated entry to less than 50% of no-compound control) and (2) % specificity > 90% (compounds that do not decrease more than 10% of AMLV control entry [residual activity greater than 90%] in comparison to no-compound control). IC_{50} (50% inhibitory concentration) was calculated using nonlinear regression analysis based on the sigmoidal dose–response equation using PRISM 8 software (GraphPad, San Diego, CA) applied to the percent inhibition and concentration data.

Thermal Shift. The interaction of compounds with the receptor binding domain (RBD) and N-terminal domain (NBD) of the SARS-CoV-2 spike was measured by differential scanning fluorimetry (DSF) using a Real-Time PCR Detection System (BioRad). Fifty μg/mL purified RBD-mFC or NBD-mFC in 50 mM HEPES (pH 7.5) and 150 mM NaCl was subjected to thermal scanning by increasing the temperature from 20 to 90 °C in the presence and absence of small molecules. We increased the temperature at 0.1 °C increments, each for 10 s incubation, and performed the thermal shift assay in triplicates for every sample. Small molecules were dissolved in DMSO and the control sample included DMSO only. SYPRO Orange protein gel stain (Invitrogen) was used at a 1:5000 v/v dilution ratio as the fluorescent probe. The inflection point of the transition curve/melting temperature (T_m) was calculated using the Boltzmann equation within Protein Thermal Shift Software.

Surface Plasmon Resonance (SPR). Multicycle SPR experiments were carried out on a Biacore S200 SPR instrument (Cytiva) equipped with an NTA series S sensor chip and equilibrated with running buffer (20 mM phosphate buffer, 2.7 mM KCl, 137 mM NaCl, 0.05% surfactant P20, pH 7.4) prepared with 1% DMSO according to established methods.[54,55]

Prior to the first cycle, the sensor chip was conditioned once with 0.35 M ethylenediamine tetraacetic acid (EDTA) for 60 s. At the beginning of each subsequent cycle, 0.5 mM $NiCl_2$ was injected for 60 s across the chip surface. Then, the recombinant 8x-His-SARS-CoV-2 spike glycoprotein (ectodomain) or 6x-His-HIV-1_{AD8} gp120 diluted in running buffer was immobilized on the sensor chip at approximately 2000 response units (RU). The analyte prepared in running buffer was injected for 180 s and allowed to dissociate for 300 s. After each concentration of analyte, the chip surface was regenerated with a 60 s injection of 0.35 M EDTA. A solvent correction curve was performed prior to the first analyte cycle and after the last analyte cycle. Response curves (Sensorgrams) were corrected for solvent variations with a DMSO solvent correction curve and were double referenced to the reference channel and zero compound (1% DMSO) blanks.

SPR data were analyzed in Biacore S200 Evaluation software (version 1.1.1), fit with a two-state kinetic binding model, and plotted in GraphPad Prism (version 9.0.1).

■ ASSOCIATED CONTENT

Supporting Information

The Supporting Information is available free of charge at https://pubs.acs.org/doi/10.1021/acsinfecdis.1c00658.

Additional experimental data (PDF)

■ AUTHOR INFORMATION

Corresponding Author

Alon Herschhorn − *Division of Infectious Diseases and International Medicine, Department of Medicine, University of Minnesota, Minneapolis, Minnesota 55455, United States; Microbiology, Immunology, and Cancer Biology Graduate Program, The College of Veterinary Medicine Graduate Program, and Institute for Molecular Virology, University of Minnesota, Minneapolis, Minnesota 55455, United States;* orcid.org/0000-0002-9323-4820; Phone: 612-3012429; Email: aherschh@umn.edu

Authors

Sneha Ratnapriya − *Division of Infectious Diseases and International Medicine, Department of Medicine, University of Minnesota, Minneapolis, Minnesota 55455, United States*

Anthony R. Braun − *Department of Biomedical Engineering, University of Minnesota, Minneapolis, Minnesota 55455, United States;* orcid.org/0000-0002-9942-3390

Héctor Cervera Benet − *Division of Infectious Diseases and International Medicine, Department of Medicine, University of Minnesota, Minneapolis, Minnesota 55455, United States*

Danielle Carlson − *Division of Infectious Diseases and International Medicine, Department of Medicine, University of Minnesota, Minneapolis, Minnesota 55455, United States*

Shilei Ding − *Centre de Recherche du CHUM; Département de Microbiologie, Infectiologie et Immunologie, Université de Montréal, Montreal, Quebec H2X 0A9, Canada*

Carolyn N. Paulson − *Department of Biomedical Engineering, University of Minnesota, Minneapolis, Minnesota 55455, United States;* orcid.org/0000-0001-8564-7345

Neeraj Mishra − *Department of Medicinal Chemistry, University of Minnesota, Minneapolis, Minnesota 55455, United States*

Jonathan N. Sachs − *Department of Biomedical Engineering, University of Minnesota, Minneapolis, Minnesota 55455, United States;* orcid.org/0000-0003-1403-5960

Courtney C. Aldrich − *Department of Medicinal Chemistry, University of Minnesota, Minneapolis, Minnesota 55455, United States;* orcid.org/0000-0001-9261-594X

Andrés Finzi − *Centre de Recherche du CHUM; Département de Microbiologie, Infectiologie et Immunologie, Université de Montréal, Montreal, Quebec H2X 0A9, Canada*

Complete contact information is available at: https://pubs.acs.org/10.1021/acsinfecdis.1c00658

Notes

The authors declare no competing financial interest.

■ ACKNOWLEDGMENTS

The authors thank the following researchers: Louis Mansky, the University of Minnesota for providing a plasmid for expression of the double mutant (K1269A H1270A) SARS-CoV-2 spike; Jason McLellan, the University of Texas at Austin for providing plasmids for expression of soluble RBD-mFC and NTD-mFC; Stefan Pöhlmann, the University of Göttingen for providing plasmids for the expression of SARS-CoV-1 and SARS-CoV-2 spikes; Fang Li, the University of Minnesota for providing the 293T-ACE2 cells; and Fatemeh Khadir, the University of Minnesota for purifying the RBD-mFC and

NTD-mFC. The authors thank the Laboratoire de Santé Publique du Québec for the live SARS-CoV-2 D614G virus and the CRCHUM BSL3 facility. The work was supported by an internal grant from the University of Minnesota Medical School to A.H. ORIP/NIH Shared Instrument Grant 1S10OD021539-01 to the ITDD/HTS Lab was used to purchase the Biacore S200 instrument. A.R.B. and J.N.S. were supported by R35 GM131814 and by a Group Grant from the Institute for Engineering in Medicine at the University of Minnesota. Work perfomed in the Finzi Lab was supported by le Ministère de l'Économie et de l'Innovation du Québec (programme de soutien aux organismes de recherche et d'innovation) and a CIHR foundation grant #352417 to A.F. A.F. is the recipient of Canada Research Chair on Retroviral Entry No. RCHS0235 950-232424.

REFERENCES

(1) Lu, R.; Zhao, X.; Li, J.; Niu, P.; Yang, B.; Wu, H.; Wang, W.; Song, H.; Huang, B.; Zhu, N.; Bi, Y.; Ma, X.; Zhan, F.; Wang, L.; Hu, T.; Zhou, H.; Hu, Z.; Zhou, W.; Zhao, L.; Chen, J.; Meng, Y.; Wang, J.; Lin, Y.; Yuan, J.; Xie, Z.; Ma, J.; Liu, W. J.; Wang, D.; Xu, W.; Holmes, E. C.; Gao, G. F.; Wu, G.; Chen, W.; Shi, W.; Tan, W. Genomic Characterisation and Epidemiology of 2019 Novel Coronavirus: Implications for Virus Origins and Receptor Binding. *Lancet* **2020**, *395*, 565−574.

(2) Kannan, S.; Ali, P. S. S.; Sheeza, A.; Hemalatha, K. COVID-19 (Novel Coronavirus 2019) - Recent Trends. *Eur. Rev. Med. Pharmacol. Sci.* **2020**, *24*, 2006−2011.

(3) Zhu, N.; Zhang, D.; Wang, W.; Li, X.; Yang, B.; Song, J.; Zhao, X.; Huang, B.; Shi, W.; Lu, R.; Niu, P.; Zhan, F.; Ma, X.; Wang, D.; Xu, W.; Wu, G.; Gao, G. F.; Tan, W. A Novel Coronavirus from Patients with Pneumonia in China, 2019. *N. Engl. J. Med.* **2020**, *382*, 727−733.

(4) Krammer, F. SARS-CoV-2 Vaccines in Development. *Nature* **2020**, *586*, 516−527.

(5) NCT04338906. Combination Therapy With Camostat Mesilate + Hydroxychloroquine for COVID-19, 2020. https://clinicaltrials.gov/show/NCT04338906.

(6) Hoffmann, M.; Kleine-Weber, H.; Schroeder, S.; Krüger, N.; Herrler, T.; Erichsen, S.; Schiergens, T. S.; Herrler, G.; Wu, N. H.; Nitsche, A.; Müller, M. A.; Drosten, C.; Pöhlmann, S. SARS-CoV-2 Cell Entry Depends on ACE2 and TMPRSS2 and Is Blocked by a Clinically Proven Protease Inhibitor. *Cell* **2020**, *181*, 271−280.e8.

(7) Bavishi, C.; Maddox, T. M.; Messerli, F. H. Coronavirus Disease 2019 (COVID-19) Infection and Renin Angiotensin System Blockers. *JAMA Cardiol.* **2020**, *5*, 745−747.

(8) Herschhorn, A.; Ma, X.; Gu, C.; Ventura, J. D.; Castillo-Menendez, L.; Melillo, B.; Terry, D. S.; Smith, A. B.; Blanchard, S. C.; Munro, J. B.; Mothes, W.; Finzi, A.; Sodroski, J. Release of Gp120 Restraints Leads to an Entry-Competent Intermediate State of the HIV-1 Envelope Glycoproteins. *mBio* **2016**, *7*, 1−12.

(9) Weitman, M.; Lerman, K.; Nudelman, A.; Major, D. T.; Hizi, A.; Herschhorn, A. Structure-Activity Relationship Studies of 1-(4-Chloro-2,5-Dimethoxyphenyl) -3-(3-Propoxypropyl)Thiourea, a Non-Nucleoside Reverse Transcriptase Inhibitor of Human Immunodeficiency Virus Type-1. *Eur. J. Med. Chem.* **2011**, *46*, 447−467.

(10) Herschhorn, A.; Gu, C.; Moraca, F.; Ma, X.; Farrell, M.; Smith, A. B.; Pancera, M.; Kwong, P. D.; Schön, A.; Freire, E.; Abrams, C.; Blanchard, S. C.; Mothes, W.; Sodroski, J. G. The B20-B21 of Gp120 Is a Regulatory Switch for HIV-1 Env Conformational Transitions. *Nat. Commun.* **2017**, *8*, No. 1049.

(11) Herschhorn, A.; Finzi, A.; Jones, D. M.; Courter, J. R.; Sugawara, A.; Smith, A. B.; Sodroski, J. G. An Inducible Cell-Cell Fusion System with Integrated Ability to Measure the Efficiency and Specificity of HIV-1 Entry Inhibitors. *PLoS One* **2011**, *6*, No. e26731.

(12) Herschhorn, A.; Marasco, Wa.; Hizi, A. Antibodies and Lentiviruses That Specifically Recognize a T Cell Epitope Derived from HIV-1 Nef Protein and Presented by HLA-C. *J. Immunol.* **2010**, *185*, 7623−7632.

(13) Harris, M.; Ratnapriya, S.; Chov, A.; Cervera, H.; Block, A.; Gu, C.; Talledge, N.; Mansky, L. M.; Sodroski, J.; Herschhorn, A. Slow Receptor Binding of the Noncytopathic HIV-2UC1 Envs Is Balanced by Long-Lived Activation State and Efficient Fusion Activity. *Cell Rep.* **2020**, *31*, No. 107749.

(14) Herschhorn, A.; Gu, C.; Espy, N.; Richard, J.; Finzi, A.; Sodroski, J. G. A Broad HIV-1 Inhibitor Blocks Envelope Glycoprotein Transitions Critical for Entry. *Nat. Chem. Biol.* **2014**, *10*, 845−852.

(15) Ratnapriya, S.; Harris, M.; Chov, A.; Herbert, Z. T.; Vrbanac, V.; Deruaz, M.; Achuthan, V.; Engelman, A. N.; Sodroski, J.; Herschhorn, A. Intra- and Extra-Cellular Environments Contribute to the Fate of HIV-1 Infection. *Cell Rep.* **2021**, *36*, No. 109622.

(16) Case, J. B.; Rothlauf, P.; Chen, R.; Liu, Z.; Zhao, H.; Kim, A.; Bloyet, L.-M.; Zeng, Q.; Tahan, S.; Droit, L.; Ilagan, M.; Tartell, M.; Amarasinghe, G.; Henderson, J.; Miersch, S.; Ustav, M.; Sidhu, S.; Virgin, H.; Wang, D.; Ding, S.; Corti, D.; Theel, E.; Fremont, D.; Diamond, M.; Whelan, S. Neutralizing Antibody and Soluble ACE2 Inhibition of a Replication-Competent VSV-SARS-CoV-2 and a Clinical Isolate of SARS-CoV-2. *Cell Host Microbe* **2020**, *28*, 475−485.

(17) Xiong, H.-L.; Wu, Y.-T.; Cao, J.-L.; Yang, R.; Ma, J.; Qiao, X.-Y.; Yao, X.-Y.; Zhang, B.-H.; Zhang, Y.-L.; Hou, W.-H.; Xu, J.-J.; Wang, S.-J.; Fu, B.-R.; Yang, T.; Ge, S.-X.; Zhang, J.; Yuan, Q.; Huang, B.-Y.; Li, Z.-Y.; Zhang, T.-Y.; Xia, N.-S. et al. Robust neutralization assay based on SARS-CoV-2 S-protein-bearing vesicular stomatitis virus (VSV) pseudovirus and ACE2-overexpressing BHK21 cells. *Emerging Microbes Infect.* **2020**, *9* (1), 2105−2113..

(18) Rogers, T. F.; Zhao, F.; Huang, D.; Beutler, N.; Burns, A.; He, W.; Limbo, O.; Smith, C.; Song, G.; Woehl, J.; Yang, L.; Abbott, R. K.; Callaghan, S.; Garcia, E.; Hurtado, J.; Parren, M.; Peng, L.; Ramirez, S.; Ricketts, J.; Ricciardi, M. J.; Rawlings, S. A.; Wu, N. C.; Yuan, M.; Smith, D. M.; Nemazee, D.; Teijaro, J. R.; Voss, J. E.; Wilson, I. A.; Andrabi, R.; Briney, B.; Landais, E.; Sok, D.; Jardine, J. G.; Burton, D. R. Isolation of Potent SARS-CoV-2 Neutralizing Antibodies and Protection from Disease in a Small Animal Model. *Science* **2020**, *369*, No. eabc7520.

(19) Yu, J.; Li, Z.; He, X.; Gebre, M. S.; Bondzie, E. A.; Wan, H.; Jacob-Dolan, C.; Martinez, D. R.; Nkolola, J. P.; Baric, R. S.; Barouch, D. H. Deletion of the SARS-CoV-2 Spike Cytoplasmic Tail Increases Infectivity in Pseudovirus Neutralization Assays. *J. Virol.* **2021**, *95*, No. e00044-21.

(20) Touret, F.; Gilles, M.; Barral, K.; Nougairède, A.; van Helden, J.; Decroly, E.; de Lamballerie, X.; Coutard, B. In Vitro Screening of a FDA Approved Chemical Library Reveals Potential Inhibitors of SARS-CoV-2 Replication. *Sci. Rep.* **2020**, *10*, No. 13093.

(21) Gruber, S. J.; Cornea, R. L.; Li, J.; Peterson, K. C.; Schaaf, T. M.; Gillispie, G. D.; Dahl, R.; Zsebo, K. M.; Robia, S. L.; Thomas, D. D. Discovery of Enzyme Modulators via High-Throughput Time-Resolved FRET in Living Cells. *J. Biomol. Screening* **2014**, *19*, 215−222.

(22) Lo, C. H.; Vunnam, N.; Lewis, A. K.; Chiu, T. L.; Brummel, B. E.; Schaaf, T. M.; Grant, B. D.; Bawaskar, P.; Thomas, D. D.; Sachs, J. N. An Innovative High-Throughput Screening Approach for Discovery of Small Molecules That Inhibit TNF Receptors. *SLAS Discovery* **2017**, *22*, 950−961.

(23) Schaaf, T. M.; Peterson, K. C.; Grant, B. D.; Thomas, D. D.; Gillispie, G. D. Spectral Unmixing Plate Reader: High-Throughput, High-Precision FRET Assays in Living Cells. *SLAS Discovery* **2017**, *22*, 250−261.

(24) Schaaf, T. M.; Peterson, K. C.; Grant, B. D.; Bawaskar, P.; Yuen, S.; Li, J.; Muretta, J. M.; Gillispie, G. D.; Thomas, D. D. High-Throughput Spectral and Lifetime-Based FRET Screening in Living Cells to Identify Small-Molecule Effectors of SERCA. *SLAS Discovery* **2017**, *22*, 262−273.

(25) Braun, A. R.; Liao, E. E.; Horvath, M.; Kalra, P.; Acosta, K.; Young, M. C.; et al. Potent Inhibitors of Toxic Alpha-Synuclein

Oligomers Identified via Cellular Time-Resolved FRET Biosensor. *npj Parkinson's Dis.* **2021**, *7*, No. 52.
(26) Wrapp, D.; Wang, N.; Corbett, K. S.; Goldsmith, J. A.; Hsieh, C.-L.; Abiona, O.; Graham, B. S.; McLellan, J. S. Cryo-EM Structure of the 2019-NCoV Spike in the Prefusion Conformation. *Science* **2020**, *367*, 1260−1263.
(27) Wong, S. K.; Li, W.; Moore, M. J.; Choe, H.; Farzan, M. A 193-Amino Acid Fragment of the SARS Coronavirus S Protein Efficiently Binds Angiotensin-Converting Enzyme 2. *J. Biol. Chem.* **2004**, *279*, 3197−3201.
(28) McKee, D. L.; Sternberg, A.; Stange, U.; Laufer, S.; Naujokat, C. Candidate Drugs against SARS-CoV-2 and COVID-19. *Pharmacol. Res.* **2020**, *157*, No. 104859.
(29) Gordon, D. E.; Jang, G. M.; Bouhaddou, M.; Xu, J.; Obernier, K.; White, K. M.; O'Meara, M. J.; Rezelj, V. V.; Guo, J. Z.; Swaney, D. L.; Tummino, T. A.; Hüttenhain, R.; Kaake, R. M.; Richards, A. L.; Tutuncuoglu, B.; Foussard, H.; Batra, J.; Haas, K.; Modak, M.; Kim, M.; Haas, P.; Polacco, B. J.; Braberg, H.; Fabius, J. M.; Eckhardt, M.; Soucheray, M.; Bennett, M. J.; Cakir, M.; McGregor, M. J.; Li, Q.; Meyer, B.; Roesch, F.; Vallet, T.; Mac Kain, A.; Miorin, L.; Moreno, E.; Naing, Z. Z. C.; Zhou, Y.; Peng, S.; Shi, Y.; Zhang, Z.; Shen, W.; Kirby, I. T.; Melnyk, J. E.; Chorba, J. S.; Lou, K.; Dai, S. A.; Barrio-Hernandez, I.; Memon, D.; Hernandez-Armenta, C.; Lyu, J.; Mathy, C. J. P.; Perica, T.; Pilla, K. B.; Ganesan, S. J.; Saltzberg, D. J.; Rakesh, R.; Liu, X.; Rosenthal, S. B.; Calviello, L.; Venkataramanan, S.; Liboy-Lugo, J.; Lin, Y.; Huang, X. P.; Liu, Y. F.; Wankowicz, S. A.; Bohn, M.; Safari, M.; Ugur, F. S.; Koh, C.; Savar, N. S.; Tran, Q. D.; Shengjuler, D.; Fletcher, S. J.; O'Neal, M. C.; Cai, Y.; Chang, J. C. J.; Broadhurst, D. J.; Klippsten, S.; Sharp, P. P.; Wenzell, N. A.; Kuzuoglu-Ozturk, D.; Wang, H. Y.; Trenker, R.; Young, J. M.; Cavero, D. A.; Hiatt, J.; Roth, T. L.; Rathore, U.; Subramanian, A.; Noack, J.; Hubert, M.; Stroud, R. M.; Frankel, A. D.; Rosenberg, O. S.; Verba, K. A.; Agard, D. A.; Ott, M.; Emerman, M.; Jura, N.; von Zastrow, M.; Verdin, E.; Ashworth, A.; Schwartz, O.; d'Enfert, C.; Mukherjee, S.; Jacobson, M.; Malik, H. S.; Fujimori, D. G.; Ideker, T.; Craik, C. S.; Floor, S. N.; Fraser, J. S.; Gross, J. D.; Sali, A.; Roth, B. L.; Ruggero, D.; Taunton, J.; Kortemme, T.; Beltrao, P.; Vignuzzi, M.; García-Sastre, A.; Shokat, K. M.; Shoichet, B. K.; Krogan, N. J. A SARS-CoV-2 Protein Interaction Map Reveals Targets for Drug Repurposing. *Nature* **2020**, *583*, 459−468.
(30) Wang, G.; Yang, M. L.; Duan, Z. L.; Liu, F. L.; Jin, L.; Long, C. B.; Zhang, M.; Tang, X. P.; Xu, L.; Li, Y. C.; Kamau, P. M.; Yang, L.; Liu, H. Q.; Xu, J. W.; Chen, J. K.; Zheng, Y. T.; Peng, X. Z.; Lai, R. Dalbavancin Binds ACE2 to Block Its Interaction with SARS-CoV-2 Spike Protein and Is Effective in Inhibiting SARS-CoV-2 Infection in Animal Models. *Cell Res.* **2021**, *31*, 17−24.
(31) Ou, X.; Liu, Y.; Lei, X.; Li, P.; Mi, D.; Ren, L.; Guo, L.; Guo, R.; Chen, T.; Hu, J.; Xiang, Z.; Mu, Z.; Chen, X.; Chen, J.; Hu, K.; Jin, Q.; Wang, J.; Qian, Z. Characterization of Spike Glycoprotein of SARS-CoV-2 on Virus Entry and Its Immune Cross-Reactivity with SARS-CoV. *Nat. Commun.* **2020**, *11*, No. 1620.
(32) Trezza, A.; Iovinelli, D.; Santucci, A.; Prischi, F.; Spiga, O. An Integrated Drug Repurposing Strategy for the Rapid Identification of Potential SARS-CoV-2 Viral Inhibitors. *Sci. Rep.* **2020**, *10*, No. 13866.
(33) Kadioglu, O.; Saeed, M.; Greten, H. J.; Efferth, T. Identification of Novel Compounds against Three Targets of SARS CoV2 Coronavirus by Combined Virtual Screening and Supervised Machine Learning. *Comput. Biol. Med.* **2021**, *133*, No. 104359.
(34) Calligari, P.; Bobone, S.; Ricci, G.; Bocedi, A. Molecular Investigation of SARS−COV-2 Proteins and Their Interactions with Antiviral Drugs. *Viruses* **2020**, *12*, No. 445.
(35) Sandrin, V.; Boson, B.; Salmon, P.; Gay, W.; Nègre, D.; Le Grand, R.; Trono, D.; Cosset, F. L. Lentiviral Vectors Pseudotyped with a Modified RD114 Envelope Glycoprotein Show Increased Stability in Sera and Augmented Transduction of Primary Lymphocytes and CD34+ Cells Derived from Human and Nonhuman Primates. *Blood* **2002**, *100*, 823−832.
(36) Zhou, Y.; Agudelo, J.; Lu, K.; Goetz, D. H.; Hansell, E.; Chen, Y. T.; Roush, W. R.; McKerrow, J.; Craik, C. S.; Amberg, S. M.; Simmons, G. Inhibitors of SARS-CoV Entry - Identification Using an Internally-Controlled Dual Envelope Pseudovirion Assay. *Antiviral Res.* **2011**, *92*, 187−194.
(37) Hoertel, N.; Sánchez-Rico, M.; Vernet, R.; Beeker, N.; Jannot, A. S.; Neuraz, A.; Salamanca, E.; Paris, N.; Daniel, C.; Gramfort, A.; Lemaitre, G.; Bernaux, M.; Bellamine, A.; Lemogne, C.; Airagnes, G.; Burgun, A.; Limosin, F. Association between Antidepressant Use and Reduced Risk of Intubation or Death in Hospitalized Patients with COVID-19: Results from an Observational Study. *Mol. Psychiatry* **2021**, *26*, 5199−5212.
(38) Lenze, E. J.; Mattar, C.; Zorumski, C. F.; Stevens, A.; Schweiger, J.; Nicol, G. E.; Miller, J. P.; Yang, L.; Yingling, M.; Avidan, M. S.; Reiersen, A. M. Fluvoxamine vs Placebo and Clinical Deterioration in Outpatients with Symptomatic COVID-19: A Randomized Clinical Trial. *JAMA* **2020**, 2292−2300.
(39) Yuan, S.; Yin, X.; Meng, X.; Chan, J. F. W.; Ye, Z. W.; Riva, L.; Pache, L.; Chan, C. C. Y.; Lai, P. M.; Chan, C. C. S.; Poon, V. K. M.; Lee, A. C. Y.; Matsunaga, N.; Pu, Y.; Yuen, C. K.; Cao, J.; Liang, R.; Tang, K.; Sheng, L.; Du, Y.; Xu, W.; Lau, C. Y.; Sit, K. Y.; Au, W. K.; Wang, R.; Zhang, Y. Y.; Tang, Y. D.; Clausen, T. M.; Pihl, J.; Oh, J.; Sze, K. H.; Zhang, A. J.; Chu, H.; Kok, K. H.; Wang, D.; Cai, X. H.; Esko, J. D.; Hung, I. F. N.; Li, R. A.; Chen, H.; Sun, H.; Jin, D. Y.; Sun, R.; Chanda, S. K.; Yuen, K. Y. Clofazimine Broadly Inhibits Coronaviruses Including SARS-CoV-2. *Nature* **2021**, *593*, 418−423.
(40) Yang, L.; Pei, R.-j.; Li, H.; Ma, X.-n.; Zhou, Y.; Zhu, F.-h.; He, P.-l.; Tang, W.; Zhang, Y.-c.; Xiong, J.; Xiao, S.-q.; Tong, X.-k.; Zhang, B.; Zuo, J.-p. Identification of SARS-CoV-2 Entry Inhibitors among Already Approved Drugs. *Acta Pharmacol. Sin.* **2021**, *42*, 1347−1353.
(41) Chen, C. Z.; Xu, M.; Pradhan, M.; Gorshkov, K.; Petersen, J. D.; Straus, M. R.; Zhu, W.; Shinn, P.; Guo, H.; Shen, M.; Klumpp-Thomas, C.; Michael, S. G.; Zimmerberg, J.; Zheng, W.; Whittaker, G. R. Identifying SARS-CoV-2 Entry Inhibitors through Drug Repurposing Screens of SARS-S and MERS-S Pseudotyped Particles. *ACS Pharmacol. Transl. Sci.* **2020**, *3*, 1165−1175.
(42) Kato, Y.; Yamada, S.; Nishiyama, K.; Satsuka, A.; Re, S.; Tomokiyo, D.; Lee, J. M.; Tanaka, T.; Nishimura, A.; Yonemitsu, K.; Asakura, H.; Ibuki, Y.; Imai, Y.; Kamiya, N.; Mizuguchi, K.; Kusakabe, T.; Kanda, Y.; Nishida, M. Clomipramine suppresses ACE2-mediated SARS-CoV-2 entry. *bioRxiv* 2021.03.13.435221..
(43) Bojadzic, D.; Alcazar, O.; Buchwald, P. Methylene Blue Inhibits the SARS-CoV-2 Spike−ACE2 Protein-Protein Interaction−a Mechanism That Can Contribute to Its Antiviral Activity Against COVID-19. *Front. Pharmacol.* **2021**, *11*, No. 2255.
(44) Yuan, S.; Yin, X.; Meng, X.; Chan, J. F. W.; Ye, Z. W.; Riva, L.; Pache, L.; Chan, C. C. Y.; Lai, P. M.; Chan, C. C. S.; Poon, V. K. M.; Lee, A. C. Y.; Matsunaga, N.; Pu, Y.; Yuen, C. K.; Cao, J.; Liang, R.; Tang, K.; Sheng, L.; Du, Y.; Xu, W.; Lau, C. Y.; Sit, K. Y.; Au, W. K.; Wang, R.; Zhang, Y. Y.; Tang, Y. D.; Clausen, T. M.; Pihl, J.; Oh, J.; Sze, K. H.; Zhang, A. J.; Chu, H.; Kok, K. H.; Wang, D.; Cai, X. H.; Esko, J. D.; Hung, I. F. N.; Li, R. A.; Chen, H.; Sun, H.; Jin, D. Y.; Sun, R.; Chanda, S. K.; Yuen, K. Y. Clofazimine Broadly Inhibits Coronaviruses Including SARS-CoV-2. *Nature* **2021**, *593*, 418−423.
(45) Braga, L.; Ali, H.; Secco, I.; Chiavacci, E.; Neves, G.; Goldhill, D.; Penn, R.; Jimenez-Guardeño, J. M.; Ortega-Prieto, A. M.; Bussani, R.; Cannatà, A.; Rizzari, G.; Collesi, C.; Schneider, E.; Arosio, D.; Shah, A. M.; Barclay, W. S.; Malim, M. H.; Burrone, J.; Giacca, M. Drugs That Inhibit TMEM16 Proteins Block SARS-CoV-2 Spike-Induced Syncytia. *Nature* **2021**, *594*, 88−93.
(46) Tummino, T. A.; Rezelj, V. V.; Fischer, B.; Fischer, A.; O'Meara, M. J.; Monel, B.; Vallet, T.; White, K. M.; Zhang, Z.; Alon, A.; Schadt, H.; O'Donnell, H. R.; Lyu, J.; Rosales, R.; McGovern, B. L.; Rathnasinghe, R.; Jangra, S.; Schotsaert, M.; Galarneau, J. R.; Krogan, N. J.; Urban, L.; Shokat, K. M.; Kruse, A. C.; García-Sastre, A.; Schwartz, O.; Moretti, F.; Vignuzzi, M.; Pognan, F.; Shoichet, B. K. Drug-Induced Phospholipidosis Confounds Drug Repurposing for SARS-CoV-2. *Science* **2021**, *373*, 541−547.
(47) Ren, J.; Zhao, Y.; Fry, E. E.; Stuart, D. I. Target Identification and Mode of Action of Four Chemically Divergent Drugs against Ebolavirus Infection. *J. Med. Chem.* **2018**, *61*, 724−733.

https://doi.org/10.1021/acsinfecdis.1c00658
ACS Infect. Dis. XXXX, XXX, XXX−XXX

(48) Ratnapriya, S.; Chov, A.; Herschhorn, A. A Protocol for Studying HIV-1 Envelope Glycoprotein Function. *STAR Protoc.* **2020**, *1*, No. 100133.
(49) Farzani, T. A.; Chov, A.; Herschhorn, A. A Protocol for Displaying Viral Envelope Glycoproteins on the Surface of Vesicular Stomatitis Viruses. *STAR Protoc.* **2020**, *1*, No. 100209.
(50) Gasser, R.; Cloutier, M.; Prévost, J.; Fink, C.; Ducas, É.; Ding, S.; Dussault, N.; Landry, P.; Tremblay, T.; Laforce-Lavoie, A.; Lewin, A.; Beaudoin-Bussières, G.; Laumaea, A.; Medjahed, H.; Larochelle, C.; Richard, J.; Dekaban, G. A.; Dikeakos, J. D.; Bazin, R.; Finzi, A. Major Role of IgM in the Neutralizing Activity of Convalescent Plasma against SARS-CoV-2. *Cell Rep.* **2021**, *34*, No. 108790.
(51) Lo, C. H.; Lim, C. K. W.; Ding, Z.; Wickramasinghe, S. P.; Braun, A. R.; Ashe, K. H.; Rhoades, E.; Thomas, D. D.; Sachs, J. N. Targeting the Ensemble of Heterogeneous Tau Oligomers in Cells: A Novel Small Molecule Screening Platform for Tauopathies. *Alzheimer's Dementia* **2019**, *15*, 1489−1502.
(52) Lo, C. H.; Pandey, N. K.; Lim, C. K. W.; Ding, Z.; Tao, M.; Thomas, D. D.; Langen, R.; Sachs, J. N. Discovery of Small Molecule Inhibitors of Huntingtin Exon 1 Aggregation by FRET-Based High-Throughput Screening in Living Cells. *ACS Chem. Neurosci.* **2020**, *11*, 2286−2295.
(53) Stroik, D. R.; Yuen, S. L.; Janicek, K. A.; Schaaf, T. M.; Li, J.; Ceholski, D. K.; Hajjar, R. J.; Cornea, R. L.; Thomas, D. D. Targeting Protein-Protein Interactions for Therapeutic Discovery via FRET-Based High-Throughput Screening in Living Cells. *Sci. Rep.* **2018**, *8*, No. 12560.
(54) Lipschultz, C. A.; Li, Y.; Smith-Gill, S. Experimental Design for Analysis of Complex Kinetics Using Surface Plasmon Resonance. *Methods* **2000**, *20*, 310−318.
(55) Karlsson, R.; Fält, A. Experimental Design for Kinetic Analysis of Protein-Protein Interactions with Surface Plasmon Resonance Biosensors. *J. Immunol. Methods* **1997**, *200*, 121−133.

https://doi.org/10.1021/acsinfecdis.1c00658
ACS Infect. Dis. XXXX, XXX, XXX−XXX